Polymer(Korea), Vol. 39, No. 3, pp. 441-452 (2015)
http://dx.doi.org/10.7317/pk.2015.39.3.441

ISSN 0379-153X(Print)
ISSN 2234-8077(Online)

2축 스크류 니더의 설계에서 스크류 로터 팁의 각도가 믹싱성능에 미치는 영향

Jing Wei†, Dabing Chen*, Dongming Zhou*, Aiqiang Zhang*, and Yuliang Yang*

The State Key Laboratory on Mechanical Transmission, Chongqing University
*School of Mechanical Engineering, Dalian University of Technology

(2014년 9월 9일 접수, 2014년 10월 31일 수정, 2014년 10월 31일 채택)

Influence of Screw Rotors Tip Angle on Mixing Performance for One Novel Twin-screw Kneader

Jing Wei†, Dabing Chen*, Dongming Zhou*, Aiqiang Zhang*, and Yuliang Yang*

The State Key Laboratory on Mechanical Transmission, Chongqing University, Chongqing, China
**School of Mechanical Engineering, Dalian University of Technology, Dalian, P. R. China*

(Received September 9, 2014; Revised October 31, 2014; Accepted October 31, 2014)

Abstract: Twin-screw kneader is an efficient polymer processing equipment. In this paper, the mixing performance of one novel intermeshing counter-rotating twin-screw kneader with different tip angles of the male rotor is simulated using the mesh superimposition technique (MST). Statistical analysis is carried out for the flow field using particle tracking technique, and distributive mixing performance is evaluated using the residence time distribution and segregation scale, while the dispersive mixing performance is estimated using the parameters such as shear rate, stretching rate and mixing index. The results show that the best distributive mixing performance is achieved when the tip angle is 0°, while the optimal dispersive mixing performance is obtained when the tip angle is 20°. The results in this paper provide a data basis for the selection of parameters and optimization of the performance for the screw rotors.

Keywords: tip angle, twin-screw kneader, rotor profiles, mixing performance.

Introduction

Kneaders are closed operation units based on a self-cleaning mechanism. Nowadays, the kneaders are widely used in blister forming and extrusion forming as well as in chemical industry, rubber industry or pharmaceutical industry for various purposes. As a continuous high efficient polymer processing mixer, especially with the rapid development of modern high polymer synthesis industries, kneaders are widely used as the core equipment of polymer reactors.[1-3]

Recently, twin-screw kneaders, as one type of kneaders, are used more and more in polymer processing. The main functions of the twin-screw kneader are self-cleaning, conveying, mixing, melting, shearing and rolling. The core component of twin-screw kneader is one pair of intermeshing screw elements. As is known to all, for the conventional screw elements of co-rotating or counter-rotating twin-screw kneaders, they have identical end cross-sections and rotate at the same speed, when the teeth number is odd, the two screw elements have the same position layout, while there is a phase difference between the screw elements when the teeth number is even. With the rapid development of the polymer industry, higher request is put forward to the twin screw kneader, such as higher melting efficiency, better mixing quality etc., while the conventional screw elements are increasingly unable to meet these requirements. Therefore, screw elements have been emphasized on and developed continuously, and different types of screw elements have been invented in recent years, such as the screw mixing element (SME), a kind of special element, was a distributive mixing promoter consisting of a standard screw profile with slots cut across the flight tip to increase leakage flow,[4] the MR, ML and MPE mixing elements manufactured by Berstorff[5] and combing mixer elements (GFM),[6] ZME/TME components,[7] *et al.*, which effectively improve the mixing quality and efficiency of the twin-screw kneader and greatly promote the development of polymer industry.

According to the current research, for traditional twin-shaft kneaders, the improvement of efficiency in intrinsic self-cleaning, transportation and mixture mechanisms is limited by the

†To whom correspondence should be addressed.
E-mail: weijing_slmt@163.com

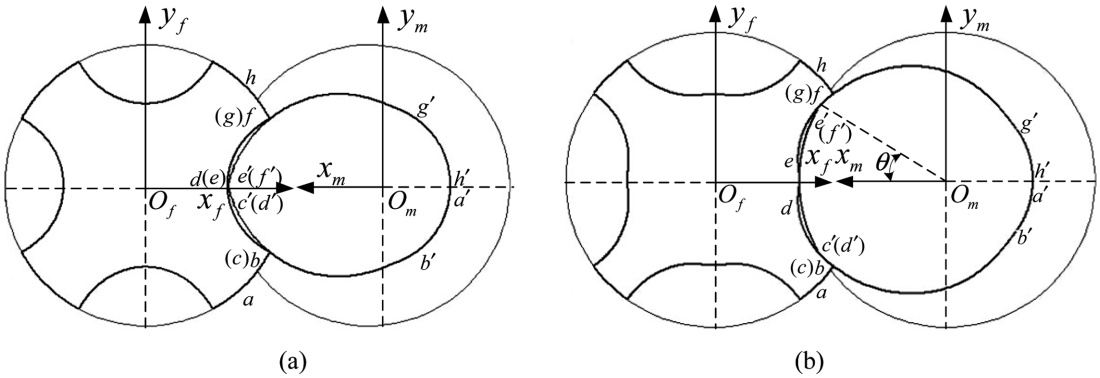

Figure 1. End cross-section of screw rotors: (a) end cross-section of screw rotors of a novel twin-screw kneader; (b) original end cross-section of screw rotors.

mechanical design itself. But these mechanisms can be improved by changing the profiles of twin-shaft kneaders based on the gear engagement theory. For screw pumps, the fill level of the plug-flow reactor depends on the intrinsic self-cleaning properties of the reactor itself. This phenomenon is well known as the "compulsory transportation effect" or "pumping effect". Based on these observations and working principles of traditional twin-screw kneaders, a novel continuous differential counter-rotating twin-screw kneader reactor, which is composed of self-cleaning, compulsory transportation and mixing and plasticizing, is proposed (Figure 1(a)), and the teeth number of the female and male rotors is four and one respectively.[8] The working principles of the twin-screw kneader are analyzed and numerical simulations for dynamic characteristics of the flow field are carried out. Three-dimensional, isothermal and steady state numerical analysis of a non-Newtonian fluid is presented based on computational fluid dynamics (CFD) theory, and the characteristics under the conditions of different speeds and center distances are studied.[9] The static loads on twin-screw kneaders were studied and a mathematical model of the force and torque moments using a numerical integration method based on differential geometry theory is presented.[10]

In actual application process, two or more polymers are usually mixed to achieve the performance requirements of the final product in order to eliminate the performance deficiencies since single polymer cannot meet with the materials performance requirements. The morphology and the specific properties of the final product depends on the uniformity of the mixture and therefore on the quality of the mixing. Mixing is comprised of distributive mixing and dispersive mixing, and distributive mixing, achieved by frequent rearrangement and reorientation, is used to describe the distribution of different components in the volume under consideration, while dispersive mixing, obtained by the shear and elongational effect, involves disaggregating or dispersing solid particles, liquid droplets, or gas bubbles. Both goals can be achieved simultaneously or in several steps in the mixer.[11]

Nowadays, two methods are widely used to study the mixing performance. The first is experimental approach, while the other is the numerical method. References 12 and 13 adopt the experimental method and the numerical method respectively to analyze the mixing performance of mixer. Due to the complexity of the flow field and the limitations of experiment, it is almost impossible to obtain all local information by using the experimental approaches, and experimental approaches are usually very expensive and time consuming. It is an effective way to study the mixing performance by using professional fluid simulation software, such as FIDAP, POLYFLOW, FLUENT. Numerical simulation methods not only have the advantages of low cost and fast speed, but also can solve those problems that are difficult to solve by experiments.

In the process of researching the mixing performance, influence of the proportion of different materials, screw speed, center distance, screw pitch and other design and process parameters on the mixing performance is usually studied by the researchers. T. Ishikawa *et al*. have evaluated the tip-clearance effect on mixing at the kneading block section of one co-rotating twin-screw extruders using 3-D numerical simulations based on finite element technique with the marker particle tracking analysis.[14] M. A. Emin *et al*.[15] have simulated the flow of plasticized maize starch in a co-rotating twin-screw extruder using computational fluid dynamic (CFD), and the flow type and profile in the extruder were discussed by using the influence of screw speed and screw configuration as exemplary process parameters. In order to determine the flow patterns in

the extruder, the governing equations were calculated by CFD software POLYFLOW, and mesh superimposition technique[16] was introduced to avoid the use of a remeshing algorithm. The mesh superimposition technique involves separately meshed flow domain, moving elements and superimposes them at time intervals with a penalty formulation of the governing equations, and the method is robust since no remeshing algorithms are needed. B. Alsteens *et al*. analyzed the effect of the material and the geometrical parameters of the kneading block, such as the stagger angle and the width of the discs, on the mixing efficiency of twin-screw extruder with three-dimensional time-dependent finite element calculations implemented by POLYFLOW, and the robustness and the accuracy of the mesh superimposition technique (MST) is evaluated.[17] J. Wei *et al.* simulated and analyzed the mixing performance of the novel twin screw kneader (illustrated in Figure 1(a)) using finite element method (FEM) combined with MST, and discussed the influence of center distance, lead and speed of rotor on the mixing performance.[18] But for the design parameter of the tip angle,[19] which directly determines the size of the screw edge region when the tip circle radius of the screw is given, not much published work is available on the analysis of its influence on the mixing performance.

In this paper, the object of this work is to evaluate the sensitivity of tip angle on the mixing performance of screw rotors for above proposed novel twin-screw kneader using FEM along with MST as implemented by POLYFLOW to calculate the residence time distribution (RTD), segregation scale, shear rates, stretching rates and mixing indexes during the mixing process.

Numerical Models and Boundary Conditions

Geometry Model. Profiles of the Female Screw Rotor: The original profiles of the end cross-section are shown in Figure 1(b), it can be seen that the profiles of the female and the male rotors are symmetric, and there are total seven segments in each end cross-section, moreover, in order to facilitate the research, the half tip angle of the male rotor, which is denoted by θ, is taken as the study object.

a) Parameter equations for *ab* and *gh* at the end cross-section of the female rotor

ab and *gh* at the end cross-section of the female rotor are two arcs with radius R_a. Parameter equation for *ab* is:

$$\begin{cases} x_{ab} = R_a \cos u_{ab} \\ y_{ab} = R_a \sin u_{ab} \end{cases} \quad \left(-\frac{\pi}{Z_f} \le u_{ab} \le u_b \right) \tag{1}$$

Parameter equation for *gh* is:

$$\begin{cases} x_{gh} = R_a \cos u_{gh} \\ y_{gh} = R_a \sin u_{gh} \end{cases} \quad \left(u_g \le u_{gh} \le \frac{\pi}{Z_f} \right) \tag{2}$$

In eqs. (1) and (2), u_b is the right boundary of u_{ab} and u_g is the left boundary of u_{gh}. Both of them can be calculated by giving the tip circle radius R_a and center distance A between the female and the male rotor.

b) Parameter equation for *bc* and *fg* at the end cross-section of the female rotor

bc and *fg* at the end cross-section of female rotor are two points, which can be expressed as:

$$\begin{cases} x_{bc} = R_a \cos u_b \\ y_{bc} = R_a \sin u_b \end{cases} \tag{3}$$

$$\begin{cases} x_{fg} = R_a \cos u_f \\ y_{fg} = R_a \sin u_f \end{cases} \tag{4}$$

(x_{bc}, y_{bc}) and (x_{fg}, y_{fg}) are the coordinates of the points *bc* and *fg*.

c) Parameter equation for *cd* and *ef* at the end cross-section of the female rotor

cd and *ef* at the end cross-section of the female rotor are two cycloids, which are formed by the track of point *c'd'* and *e'f'* at the end cross-section of the male rotor. Parameter equation for *cd* is:

$$\begin{cases} x_{cd} = -x_{c'd'} \cos k_{fm} u_{cd} - y_{c'd'} \sin k_{fm} u_{cd} + A \cos i_{fm} u_{cd} \\ y_{cd} = -x_{c'd'} \cos k_{fm} u_{cd} + y_{c'd'} \sin k_{fm} u_{cd} + A \sin i_{fm} u_{cd} \end{cases} \quad (u_c \le u_{cd} \le u_d) \tag{5}$$

(x_{cd}, y_{cd}) and ($x_{c'd'}$, $y_{c'd'}$) are the coordinates of the points of *cd* and *c'd'*, and $x_{c'd'} = -R_a \cos\theta$, $y_{c'd'} = -R_a \sin\theta$, $i_{fm} = Z_m/Z_f$, $k_{fm} = i_{fm}+1$, Z_m and Z_f are the teeth number of male rotor and female rotor respectively.

Parameter equation for *ef* is:

$$\begin{cases} x_{ef} = -x_{e'f'} \cos k_{fm} u_{ef} - y_{e'f'} \sin k_{fm} u_{ef} + A \cos i_{fm} u_{ef} \\ y_{cd} = -x_{e'f'} \cos k_{fm} u_{ef} + y_{e'f'} \sin k_{fm} u_{ef} + A \sin i_{fm} u_{ef} \end{cases} \quad (u_e \le u_{ef} \le u_f) \tag{6}$$

(x_{ef}, y_{ef}) and ($x_{e'f'}$, $y_{e'f'}$) are the coordinates of points *ef* and *e'f'*, and $x_{e'f'} = -R_a \cos\theta$, $y_{e'f'} = R_a \sin\theta$.

d) Parameter equations for *de* at the end cross-section of the female rotor

de at the end cross-section of the female rotor is a section of

arc with radius $A-R_a$. Parameter equation for de is:

$$\begin{cases} x_{de} = (A-R_a)\cos u_{de} \\ y_{de} = (A-R_a)\sin u_{de} \end{cases} \quad (u_d \le u_{de} \le u_e) \tag{7}$$

(x_{ed}, y_{de}) are the coordinates of the points of de.

Profiles of the Male Screw Rotor: a) Parameter equations for $a'b'$ and $g'h'$ at the end cross-section of the male rotor

$a'b'$ and $g'h'$ at the end cross-section of male rotor are two arcs with radius $A-R_a$. Parameter equation of $a'b'$ is:

$$\begin{cases} x_{a'b'} = (A-R_a)\cos u_{a'b'} \\ y_{a'b'} = (A-R_a)\sin u_{a'b'} \end{cases} \quad \left(-\frac{\pi}{Z_m} \le u_{a'b'} \le u_{b'}\right) \tag{8}$$

Parameter equation for $g'h'$ is:

$$\begin{cases} x_{g'h'} = (A-R_a)\cos u_{g'h'} \\ y_{g'h'} = (A-R_a)\sin u_{g'h'} \end{cases} \quad \left(u_{g'} \le u_{g'h'} \le \frac{\pi}{Z_m}\right) \tag{9}$$

$(x_{a'b'}, y_{a'b'})$ and $(x_{g'h'}, y_{g'h'})$ are the coordinates of the points of $a'b'$ and $g'h'$.

b) Profile for $b'c'$ and $f'g'$ at the end cross-section of the male rotor

$b'c'$ and $f'g'$ at the end cross-section of the male rotor are two cycloids, which are formed by the track of points bc and fg at the end cross-section of the female rotor. Parameter equation for $b'c'$ is:

$$\begin{cases} x_{b'c'} = -x_{bc}\cos k_{mf}u_{b'c'} - y_{bc}\sin k_{mf}u_{b'c'} + A\cos i_{mf}u_{b'c'} \\ y_{b'c'} = -x_{bc}\cos k_{mf}u_{b'c'} + y_{bc}\sin k_{mf}u_{b'c'} + A\sin i_{mf}u_{b'c'} \end{cases} \quad (u_{b'} \le u_{b'c'} \le u_{c'}) \tag{10}$$

(x_{bc}, y_{bc}) and $(x_{b'c'}, y_{b'c'})$ are the coordinates of the points of bc and $b'c'$, $i_{mf} = Z_f/Z_m$, $k_{mf} = i_{mf}+1$, Z_m and Z_f are the teeth number of male rotor and female rotor respectively.

Parameter equation for $f'g'$ is:

$$\begin{cases} x_{f'g'} = -x_{fg}\cos k_{mf}u_{f'g'} - y_{fg}\sin k_{mf}u_{f'g'} + A\cos i_{mf}u_{f'g'} \\ y_{f'g'} = -x_{fg}\cos k_{mf}u_{f'g'} + y_{fg}\sin k_{mf}u_{f'g'} + A\sin i_{mf}u_{f'g'} \end{cases} \quad (u_{f'} \le u_{f'g'} \le u_{g'}) \tag{11}$$

(x_{fg}, y_{fg}) and $(x_{f'g'}, y_{f'g'})$ are the coordinates of the points of fg and $f'g'$.

c) Parameter equation for $c'd'$ and $e'f'$ at the end cross-section of the male rotor

$c'd'$ and $e'f'$ at the end cross-section of male rotor are two points, which can be expressed as:

$$\begin{cases} x_{c'd'} = R_a\cos u_{d'} \\ y_{c'd'} = R_a\sin u_{d'} \end{cases} \tag{12}$$

$$\begin{cases} x_{e'f'} = R_a\cos u_{e'} \\ y_{e'f'} = R_a\sin u_{e'} \end{cases} \tag{13}$$

$(x_{c'd'}, y_{c'd'})$ and $(x_{e'f'}, y_{e'f'})$ are the coordinates of the points $c'd'$ and $e'f'$. And $u_{d'} = \pi + \theta$, $u_{e'} = \pi - \theta$.

d) Parameter equation for $d'e'$ at the end cross-section of the male rotor

$d'e'$ at the end cross-section of the male rotor is a section of arc with radius R_a. Parameter equation for $d'e'$ is:

$$\begin{cases} x_{d'e'} = R_a\cos u_{d'e'} \\ y_{d'e'} = R_a\sin u_{d'e'} \end{cases} \quad (u_{d'} \le u_{d'e'} \le u_{e'}) \tag{14}$$

$(x_{d'e'}, y_{d'e'})$ are the coordinates of the points of $d'e'$. And $u_{d'} = \pi + \theta$, $u_{e'} = \pi - \theta$.

Evolution of the Profiles at the End Cross-section of the Rotors: When the tip angle θ is 0°, $c'd'$, $d'e'$, $e'f'$ at the end cross-section of the male rotor merge into a point $c'f'$, whose coordinate is $(R_a, 0)$, meanwhile, arc de at the end cross-section of the female rotor turn into a point whose coordinate is $(A-R_a, 0)$, and together with cd, ef merge into a new cycloid cf, which is exactly formed by the track of point $c'f'$. The final end cross-section is just the end cross-section as shown in Figure 1(a), and at this time, parameter equation for cf is:

$$\begin{cases} x_{cf} = -R_a\cos k_{fm}u_{cf} + A\cos i_{fm}u_{cf} \\ y_{cf} = -R_a\sin k_{fm}u_{cf} + A\sin i_{fm}u_{cf} \end{cases} \quad (u_c \le u_{cf} \le u_f) \tag{15}$$

(x_{cf}, y_{cf}) are the coordinates of the points of cf.

Properties and forming methods of other segments of the profiles have no change, and various profiles at the end cross-section can be obtained when giving different non-vanishing tip angles.

Geometry Model of the Screw Rotors: When the profiles at the end cross-section of female and male rotors rotate along their center axes with a certain lead, a three-dimensional solid model of the screw rotors can be obtained. The parametric equations of a right-directional helicoid can be expressed as:

$$\begin{cases} x = x(t)\cos\tau - y(t)\sin\tau \\ x = x(t)\sin\tau + y(t)\cos\tau \\ z = P\tau \\ P = S2/2\pi \end{cases} \tag{16}$$

where, $(x(t), y(t))$ are the coordinates of the profiles at the end cross-section of female and male rotors. τ is a parametric variable, which shows the rotation angle from the initial position to the end position along axis z, S is the lead of the screw

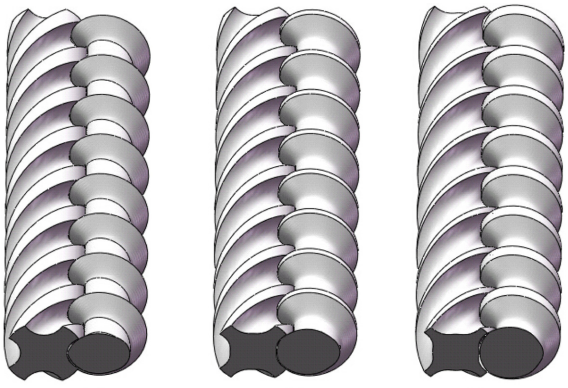

Figure 2. Geometry models of the screw rotors: (a) $\theta = 0^{o}$; (b) $\theta = 20^{o}$; (c) $\theta = 40^{o}$.

rotors, for male and female rotor, S is S_M and S_F, respectively. Here the clockwise direction is taken as the positive value, and for left-directional helicoid, the positive sign in front of τ in the equations of x and y needs to be changed to negative sign. According to the equations of helicoid and the coordinates of the profiles at the end cross-section of the rotors, the 3D model of the female and male rotors can be obtained.

Figure 2 shows the geometry models of female and male rotors when the tip angle is 0°, 20°, and 40°, respectively. With the increasing of tip angle θ, dimension of the screw groove increases and the size of the screw edge region decreases gradually of the female rotor, while the male rotor is opposite. So it is clear that tip angle of the male rotor directly affects the dimensions of screw groove and screw edge region, which are the important parameters in the design of screw rotors. Therefore, in order to design screw rotors with reasonable structure and ideal performance, study of the relationship between the tip angle and the mixing performance will be helpful.

In this paper, five groups of tip angles are selected, which are 0°, 10°, 20°, 30°, and 40°, respectively, to implement the comparative analysis of the mixing performance of screw rotors.

Finite Element Model. POLYFLOW is a finite element computational fluid dynamics (CFD) program designed primarily for simulating applications where viscous and viscoelastic flows play an important role. The flows can be isothermal or non-isothermal, two or three-dimensional, steady-state or time-dependent. POLYFLOW is usually used to solve flow problems in polymer and rubber processing, food rheology, glass-work furnaces, and many other rheological applications, and it has a wide variety of fluid models and enough constitutive models available.

After building the geometry models of screw rotors and flow channel, finite element mesh generation and specifying of the boundary and region types are done by GAMBIT, the pre-processor of POLYFLOW. In order to facilitate comparison, the identical method of mesh generation is applied in different tip angels. Since the simulation process used is the transient analysis, POLYFLOW will remesh the rotors and flow channel at each time step using MST. Figure 3 shows the finite element models of screw rotors and flow channel at $\theta = 0^{o}$, the left female screw rotor and the right male rotor has 145383 and 105140 tetrahedral elements, respectively, while there are a total of 128000 hexahedron elements in the flow channel region with a three-layer boundary layer that has a thick equal to the clearance between the screw rotor and flow channel, and the intermeshing area has been refined in order to obtain a good result.

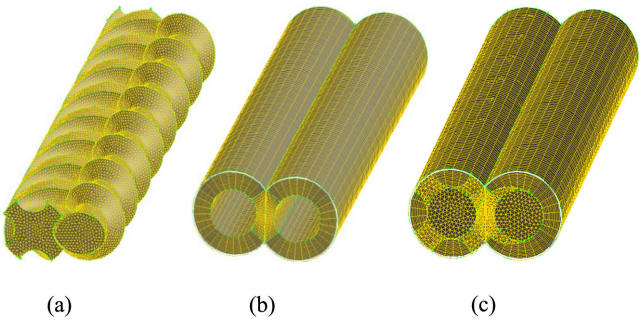

Figure 3. Finite element models: (a) screw rotors; (b) flow channel; (c) superimposed screw rotors and channel.

Mathematical Model and Boundary Conditions. In the simulation process of flow field, taking the specific process conditions of melt conveying section and polymer properties into account, following assumptions are made:[20]

(1) Material is fully filled in the entire flow channel.

(2) The fluid flow is isothermal, that is all the points have the same temperature in the flow field.

(3) The flow is laminar flow, and the Reynolds number is very small.

(3) Volume force, such as inertial force, gravity, is negligible, because it's much smaller than the viscous force.

(5) The fluid is incompressible.

(6) There is no-slip on the wall of flow channel.

Based on the above assumptions, continuity equation, momentum equation and constitutive equation are given respectively to describe the fluid.

Continuity equation:

$$\nabla \cdot v + \frac{\beta}{\eta}\Delta p = 0 \tag{17}$$

Momentum equation:

$$H(v-\bar{v})+(1-H)(-\nabla p+\nabla\cdot T+\rho g-\rho a)=0 \quad (18)$$

Constitutive equation:

$$T=2\eta D \quad (19)$$

where, ∇ is the Hamilton operator, v is the velocity vector, β is the relative compression factor, default is 0.01 in POLYFLOW, η is the apparent viscosity, p is the pressure, H is a step function, value is 0 or 1, $\bar{v}$ is the local velocity of moving parts, T is the extra-stress tensor, ρ is the density of material, ρg is the volume force, ρa is the acceleration term, D is the rate of deformation tensor.

The fluid is the generalized fluid and its constitutive equation follows Bird-Carreau model, which can be expressed as:[21]

$$\eta(\dot{\gamma})=\eta_\infty+(\eta_0-\eta_\infty)(1+(\lambda\dot{\gamma})^2)^{(n-1)/2} \quad (20)$$

where, η_∞ is infinite shear rate viscosity, and its value is zero, η_0 is zero shear rate viscosity, λ is the natural time, n is the power-law index.

In the simulation, physical parameters of HDPE, which is: η_0=2100 pa·s, η=0.07 s, n=0.58, are used.

During the simulation, the female rotor rotates counterclockwise while the male rotor rotates clockwise, and the rotational speeds of them are 25 and 100 rpm, respectively. Since the rotation angle of male and female rotors are set as 9° and 36°, respectively each time, so the time step is 0.06 s. In the analysis process, the screw rotors are considered as the moving parts, due to no slip of the screw surface, so the melt speed of the screw surface is the same as that of the screw surface. As the barrel is a fixed component, so the speed of the outer wall of the flow channel which coincides with the barrel inner surface is zero. Inlet and outlet, of the channel adopt the differential pressure boundary condition, that is $\Delta P=P_o-P_I$, and in the CFD software POLYFLOW, it is required to specify the pressure of inlet and outlet, respectively, meanwhile, in this paper the purpose is to study the mixing performance in different tip angles of one novel twin-screw kneader whose pressure difference is 5.0 MPa, and the inlet and outlet pressure is set as 0 and 5.0 MPa in the simulation, respectively.

Results and Discussion

Spatial Flow Pattern of Particles in the Flow Channel. For the dynamic simulation of mixing process, the lead of male rotor is 50 mm, rotation speed is 100 rpm, since the ratio of teeth number of female and male rotors is four to one, the lead of female rotor is 200 mm and revolving speed is 25 rpm, center distance between the axes of female rotor and male rotor is 50.4 mm. According to the simulation results, spatial flow patterns of particles in different tip angles are consistent, and here the spatial flow pattern when the tip angle is 0° is given to describe this process.

At t = 0 s, 1500 particles were evenly placed initially in the inlet of the flow channel, and these particles are considered to be massless points such that their presence does not affect the flow field and interactions among particles, such as Van der Waals attraction forces and friction are ignored.[22] In order to facilitate the observation of particles mixing, a concentration field is created in the entry section, because there is no diffusion and chemical reactions between the particles, so the concentration of any particle is a constant, and the particles in the upper part of the inlet have a concentration 1 and their colors are red, while the particles in the lower part have a concentration 0 and their colors are blue. With the rotation of the screw rotors, tracer particles flow from inlet to outlet in the flow channel gradually. Figure 4 records the movement situation of the particles from t = 0 s to t = 5.88 s. At t = 0.42 s, it can be seen that the particles are pushed forward with the rotation of the screw rotors, meanwhile, it exists a mutual exchange of particles between the upper and lower part during the movement, but it is not obvious. At t = 0.84 s, we find that there are more blue particles moving into the upper part of the right side of the channel, but almost no particles move into the upper part of the left side of the channel, which is mainly because the rotational speed of male screw is significantly higher than that of the female screw, so the blue particles move into the upper part from the lower part of the channel in a shorter time under the driving of the male rotor. At t = 1.26 s, some blue particles have moved into the upper part of the left side of the channel, which is rather obvious when t = 1.68 s. As the time goes on, tracer particles continue to move in the flow channel and the particle exchange is more intensified. At t = 4.62 s, some tracer particles have reached the end of the flow channel and outflow from the outlet. At t = 5.88 s, the two kinds of particles have achieved the ideal mixing effect, and the particles outflow from the outlet have reached a better mixing state. The spatial flow pattern of particles in the flow channel indicates that particles not only exist the axial movement in the flow channel, but also there is cross flow between the upper and lower part. Therefore, the particles continuously

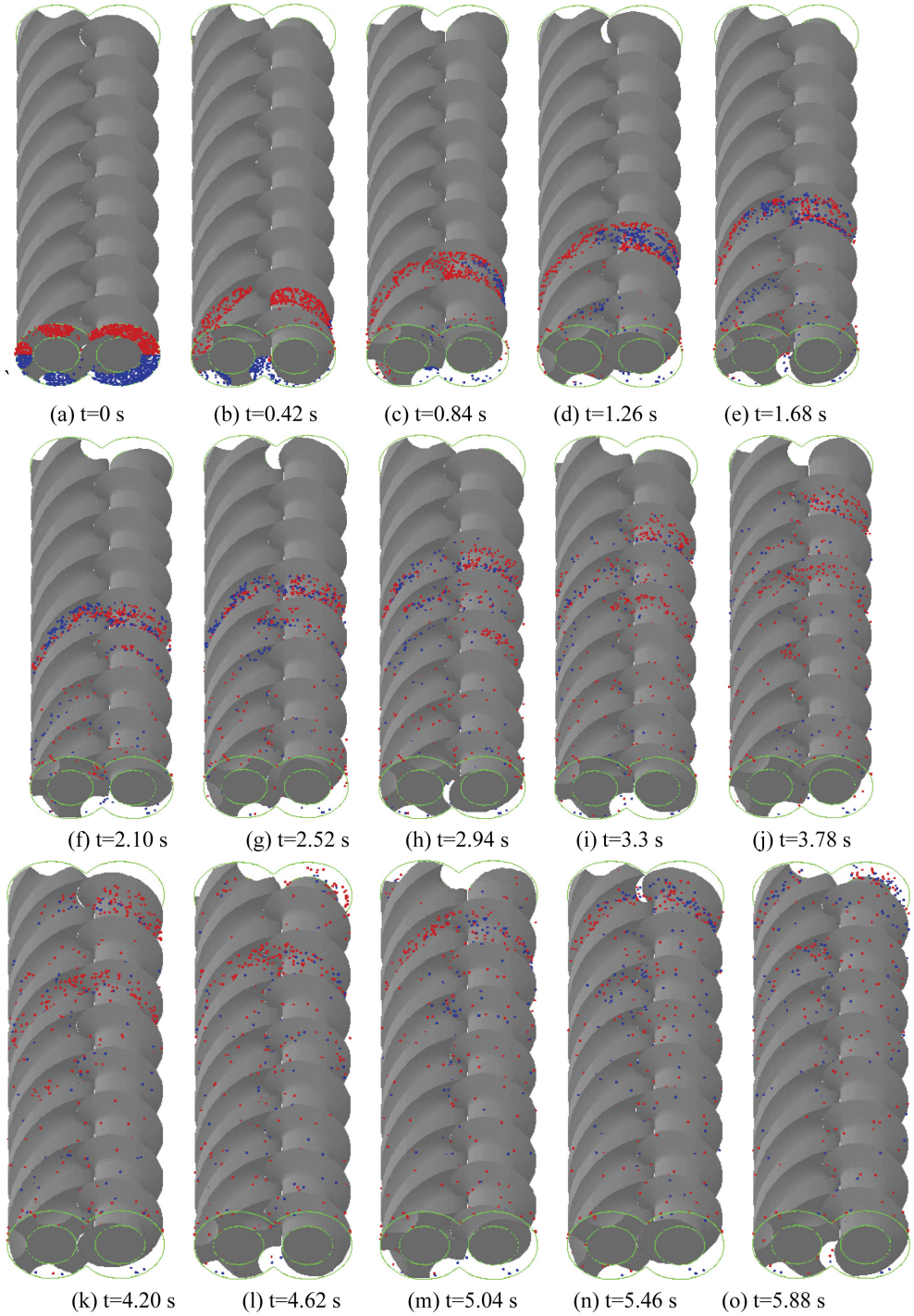

Figure 4. Spatial flow pattern of particles.

exchange between the two sides of the flow channel, which can improve the distributive mixing capability.

Trajectories of Particles. It is very important to investigate the particle trajectories for comprehensively understanding the conveying and mixing mechanism for materials in the process of studying the mixing ability of the twin-screw kneader. Through the analysis of particle trajectories, it can basically determine the process of conveying and mixing of material. Generally, most researchers implement the experiment observation by transparent barrel made of high polymer material or

the observation window which is set up on the barrel, meanwhile, tracer material is added to obtain the information of conveying and mixing. With the development of CFD technique, we can use computer simulation technology to carry out the visualization research of particle trajectories in polymer processing.

In this paper, visualization research of particle trajectories is implemented by using the computational fluid dynamics software POLYFLOW. In order to obtain the trajectories of particles in the flow channel, first of all it needs to calculate the velocity field by defining and solving the Navier-Stokes equations in the fluid region, and then we can obtain the particle trajectories through integral the velocity vector on time. As can be seen in Figure 5, both red and blue tracer particles exist four types of trajectories, as shown in Figure 5(a), (b), (c), (d) and Figure 5(e), (f), (g), (h), respectively. Moreover, the four types of trajectories can be divided into two categories, of which the first is that the particle trajectories pass through only one side of the channel, as shown in Figure 5(a), (b), (e), (f), the other is that the particle trajectories pass through both sides of the channel, as shown in Figure 5(c), (d), (g), (h), and most of the particle trajectories belong to the latter. For each category, some of the particle trajectories are relatively simple, while others are complicated, and to a certain extent, the more complex the particle trajectory is, the more fully it mixes. Based on the particle trajectories, it can be clearly seen that tracer particles exist circulation and back flow patterns along the screw rotors in the whole flow channel, which is mainly due to the back pressure. Significantly, circulation and back flow is beneficial to the mixing of materials, but the residence time of particles will increase. Meanwhile, it is noteworthy that in the process of visualization research of the particle trajectories, almost no particle trajectories are found only pass through the left side of the channel, which is mainly because the rotational speed of the female screw is low in the mixing process, leads to the particles in the left side of the channel have a higher chance to be dragged into the right side of the channel by the male rotor with a high speed. Thus, it is clear that the male screw plays an important role in the mixing process.

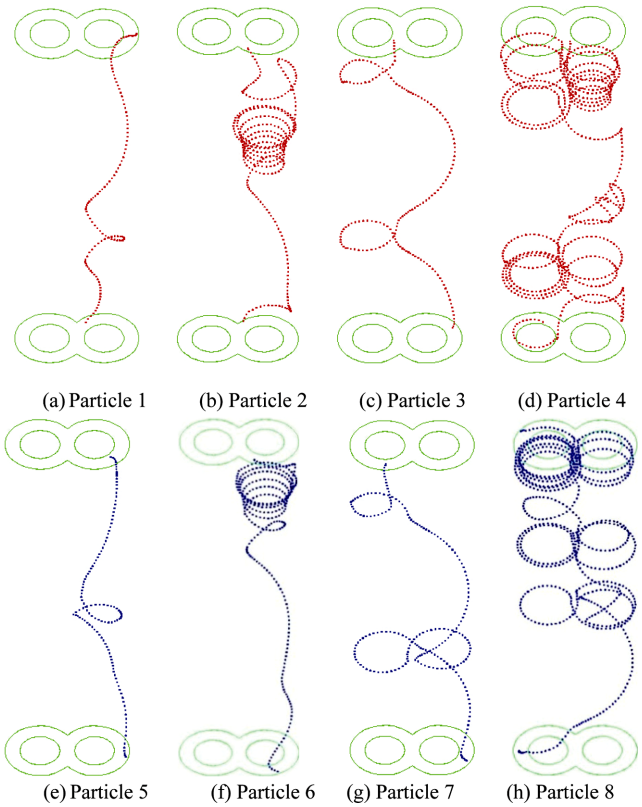

Figure 5. Trajectories of particles.

In order to study the mixing performance of screw rotors in different tip angles, statistical analysis was carried out for flow field using particle tracking technique to obtain the parameters along the particle trajectories, such as the residence time, segregation scale, shear rate, stretching rate, and the mixing index, to estimate the distributive and dispersive mixing performance of the screw rotors.

Evaluation of Distributive Mixing Performance with RTD. Residence time distribution (RTD) is an important indicator to measure the distributive mixing performance.[23] The residence time is usually used to describe the time history of a fluid inside a reactor. As the trajectories and the velocities along these trajectories are often different for the particles, so the residence time is not unique, and the longer the residence time is, the better the mixing effect is. Comparing the RTD curves under different tip angles can directly reflect the effect of distributive mixing under different conditions. The residence time distribution function and the cumulative residence time distribution function are given by eqs. (21) and (22).

$$E(t) = \frac{C}{\int_0^\infty C dt} \cong \frac{C}{\sum_0^\infty C\Delta t} \tag{21}$$

$$F(t) = \int_0^t E(t)dt \cong \frac{\sum_0^t C\Delta t}{\sum_0^\infty C\Delta t} \tag{22}$$

where, C is the concentration of the tracer at the exit at time t, Δt is the time step.

Figure 6 shows the RTD curves under different tip angles, as can be seen from the graph, the residence time of particles mainly concentrate in the convex region. When the tip angle is 40°, the convex part of the RTD curve is in the leftmost, followed by 30°, and the deviation extent of the bulges of RTD curve under other tip angles is relatively consistent. Moreover, the closer the bulge tends to the left, the shorter the residence time of most particles is, so we can preliminary judge that the distributive mixing capability is poor when the tip angle is 30° and 40°.

In order to facilitate the quantitative analysis of residence time distribution, time of 90 percent of the particles outflow the channel under different tip angles, which is denoted by T_{90}, is counted. As shown in Figure 7, it can be seen that T_{90} is the longest when the tip angle is 0°, which indicates that the particles have experienced a quite long mixing process, and the distributive mixing ability is good, followed by 10° and 20°, when the tip angle is 30° and 40°, especially 40°, the corresponding value of T_{90} is small, from which we can judge that the distributive mixing ability is poor when the tip angle is 30° and 40°, and it is consistent with the above analysis results.

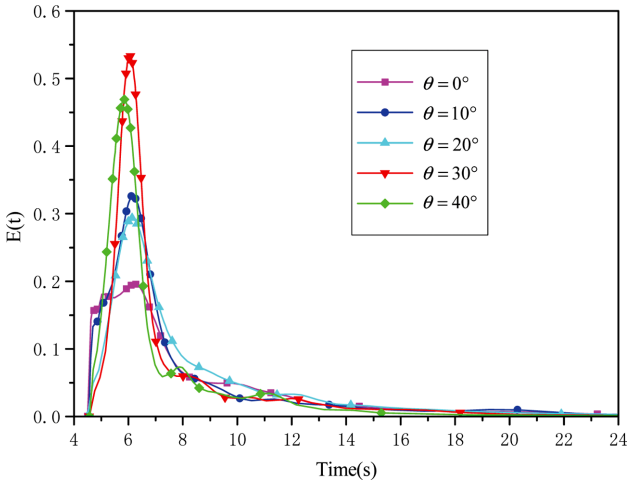

Figure 6. RTD curves in different tip angles.

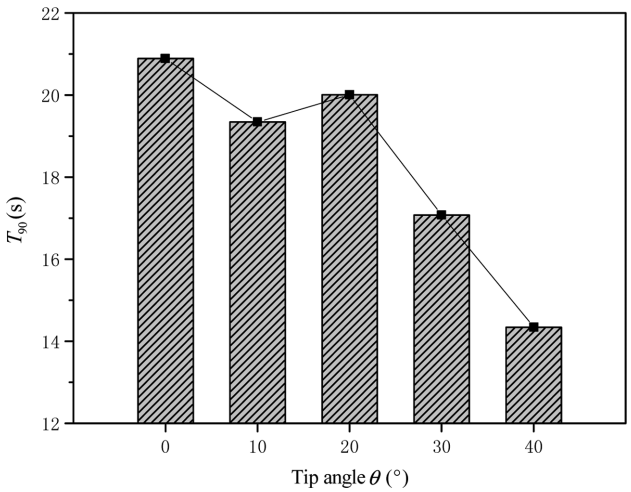

Figure 7. T_{90} in different tip angles.

Evaluation of Distributive Mixing Performance with Segregation Scale. Segregation scale is another important parameter in estimating the distributive mixing performance.[24] In the process of describing the spatial flow pattern of particles, we defined the particles with a concentration 1 in the upper part of the channel inlet, while a concentration 0 in the lower part. Now, let c denotes the concentration of particles in the mixing process, and its evolution is governed by $c^{\&}=0$.

At time t, consider a set of M pairs of particles separated by a distance r. For the j-th pair and time t, let c'_j and c''_j denote the concentrations at both particles of the pair, moreover, let $\bar{c}$ denotes the average concentration of all particles and σ_c the standard deviation. At time t, the correlation coefficient $R(r, t)$ for the concentration is defined as follows:

$$R(r,t) = \frac{\sum_{j=1}^{M} (c'_j - \bar{c}) \cdot (c''_j - \bar{c})}{M\sigma_c^2} \tag{23}$$

The function $R(r, t)$ gives the probability of finding a pair of random particles with a relative distance r and with the same concentration. Let ξ be such that $R(\xi, t)=0$, when $r = \xi$, it cannot predict whether the members of the pair have the same concentration or not. The segregation scale $S(t)$ is defined as shown in eq. (24).

$$S(t) = \int_0^{\xi} R(r,t)dr \tag{24}$$

In eq. (24), $S(t)$ is a measure of the size of the regions of homogeneous concentration, and $S(t)$ decreases when mixing improves.

Curves of segregation scale changing with time in different tip angles are shown in Figure 8. As can be seen, in the initial stage, the segregation scale gradually become smaller with time, after about 6 s, the curves of segregation scale corresponding to 20°, 30° and 40° appeare to fluctuate, and the values of segregation scale increases obviously, which indicate that particle accumulation phenomenon has emerged in the mixing process, and this phenomenon is not conducive to the distributive mixing of particles. When the tip angle is 0° and 10°, the segregation scale curves also have the rising trend, but

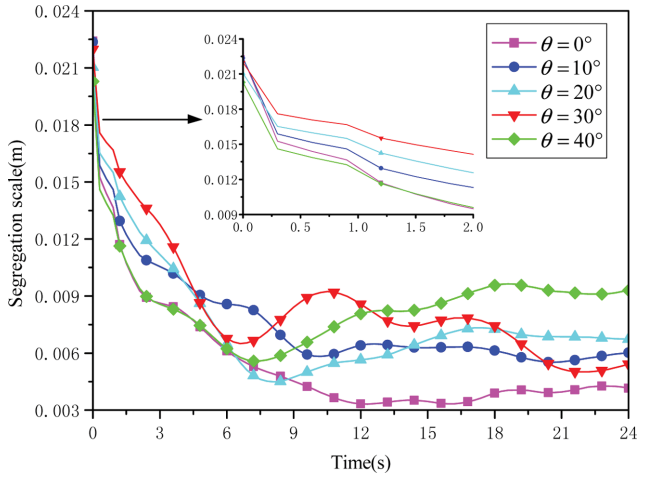

Figure 8. Curves of segregation scale in different tip angles.

finally tend to be stable, and the value is small.

Based on the above analysis, the comprehensive judgment is obtained that when the tip angle is smaller than 20°, the distributive mixing ability of screw rotors is better than that while the tip angle is greater than 20°, and the best distributive mixing ability of screw rotor can be achieved when the tip angle is 0°.

Evaluation of Dispersive Mixing Performance with Shear Rate and Stretching Rate. Sizes of material particles decrease continuously in the dispersive mixing process, and the shear rate and stretching rate plays a major role in the process, the larger shear rate and stretching rate can effectively promote the dispersion of particles. Figure 9 shows the probability density function curves of maximum shear rate and stretching rate respectively, and it can be seen that this two set of curves have the similar distribution trend respectively, but it's important to note the difference of peak in each set of curves, for example, when the tip angle is 20°, its corresponding peak is the smallest in each set of curves, which means at this time the number of particles with low maximum shear rate and stretching rate is the least, so there will be many particles subject to a high maximum shear rate and stretching rate, and the dispersive mixing performance will be better.

In order to study the overall dispersive mixing performance of screw rotors in different tip angles, the average of maximum shear rate and stretching rate is solved. As shown in Figure 10, it can be seen that when the tip angle is 20°, its corresponding value is obviously higher than that in other angles, which indicates that the particles have subjected to a stronger shear and stretching effect at this time, and the dispersive mixing performance of the screw rotor will be better. Moreover, when the

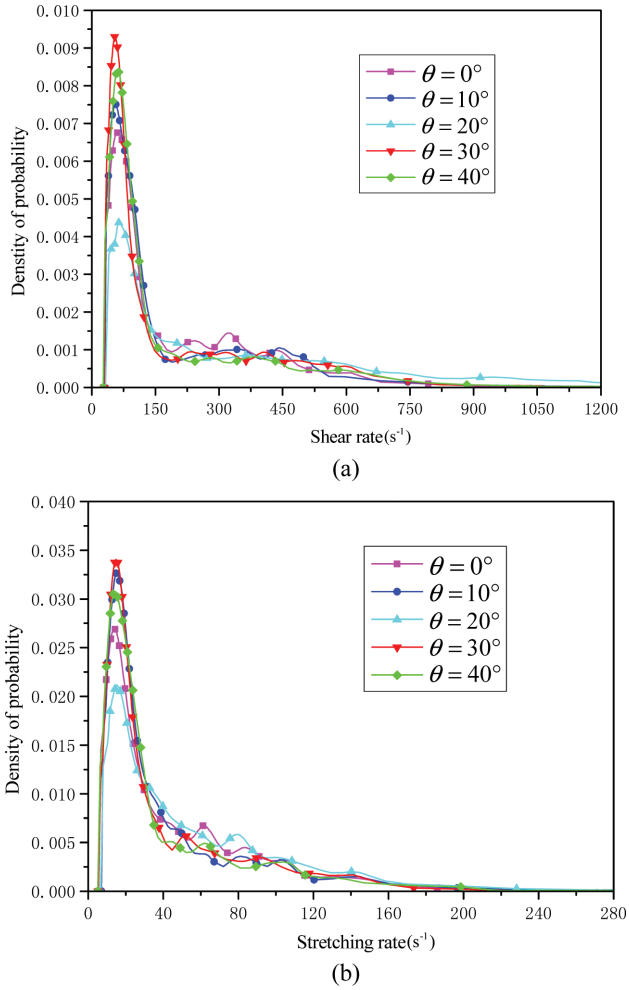

Figure 9. Probability density function in different tip angles: (a) maximum shear rate; (b) maximum stretching rate.

tip angle is less than 20°, the corresponding value is higher than that when the tip angle is greater than 20°, which indicates that when the tip angle is less than 20°, the particles have experienced higher shear and stretching effect in the mixing process, and the difference of dispersive mixing performance in different tip angles will be further discussed below.

Evaluations of Dispersive Mixing Performance with Mixing Index. In order to further study the dispersive mixing performance of the screw rotors, the parameter of mixing index, which is introduced by Cheng and Manas-Zloczower [25] and can be considered to be a mapping of the mechanism of dispersive mixing within the kneader, is used to evaluate the flow characteristics of flow field. Its definition is shown in eq. (25):

$$\lambda = \frac{|D|}{|D|+|W|} \tag{25}$$

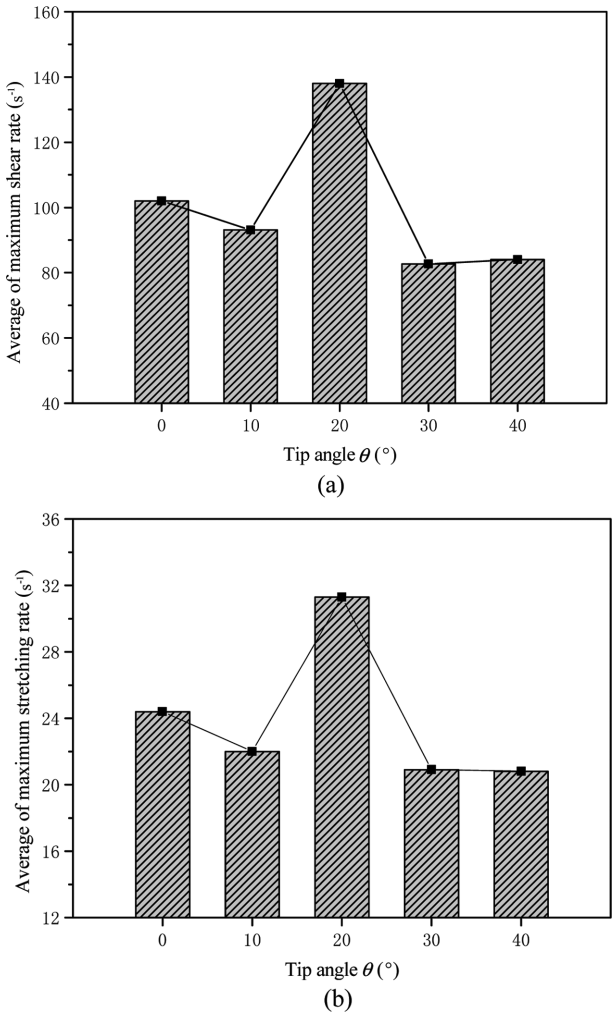

Figure 10. Averages in different tip angles: (a) maximum shear rate, (b) maximum stretching rate.

where, D is the rate of strain tensor and W is the vorticity tensor, which are the symmetric and asymmetric components of the velocity gradient tensor. For a mixing index of 0, the system is undergoing purely rotational flow and no effective mixing can occur, and a mixing index 0.5 denotes simple shear flow, while a value of 1.0 denotes elongational flow, and elongational flow is more effective than the simple shear flow in the process of dispersive mixing.[26]

Similarly, the average of the maximum mixing index is calculated to estimate the overall dispersive mixing ability of screw rotor in different tip angles. As shown in Figure 11, we can see that when the tip angle is 20°, its corresponding value is the maximum, which indicates that the dispersive mixing performance is the best at this time, and it is consistent with the above analysis. Moreover, when the tip angle is less than 20°, its corresponding value is lower than that while the tip angle is

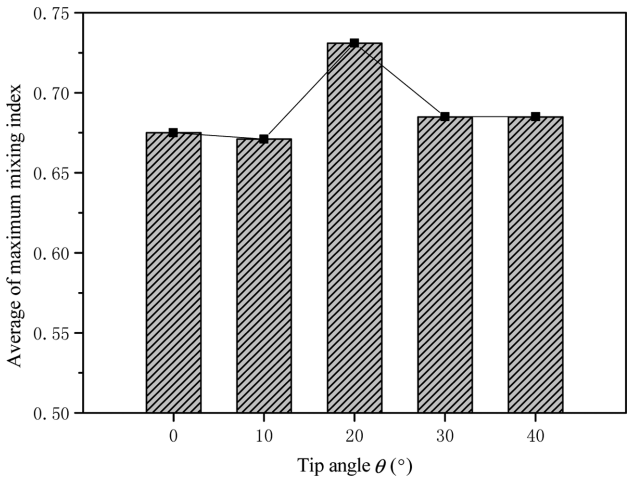

Figure 11. Average of maximum mixing index in different tip angles.

greater than 20°, which is opposite to the change trend shown in Figure 10, and it shows that when the screw angle is less than 20°, the proportion of shear flow the particles experienced is higher than that while the tip angle is greater than 20°.

Conclusions

In this paper, the mixing performance of the screw rotors for one novel intermeshing counter-rotating twin-screw kneader in different tip angles is analyzed using FEM along with MST implemented by POLYFLOW. Particle tracking technique is used to obtain the parameters along the particle trajectories, such as the residence time, segregation scale, shear rate, stretching rate, and the mixing index, and then statistical analysis is carried out to estimate the distributive and dispersive mixing performance of the screw rotors. The conclusions are as followings:

1. The spatial flow pattern and trajectories of the particles indicate that particles not only exist the axial movement in the mixing process, but also cross flow between the upper and lower part of the flow channel. Therefore, the particles continuously exchange between the two sides of the flow channel, which can improve the distributive mixing capability, and for the screw rotors, the male screw with a high rotating speed plays an important role in the mixing process.

2. In the process of statistical analysis, distributive mixing performance is estimated using the RTD and the segregation scale, while the dispersive mixing performance is evaluated using the average of the maximum shear rate and stretching rate as well as the mixing index. The results show that, when

the tip angle is smaller than 20°, the distributive mixing performance of the screw rotors is better than that while the tip angle is greater than 20°, and the best distributive mixing performance can be achieved when the tip angle is 0°, for the dispersive mixing, although when the tip angle is less than 20°, the particles have experienced higher shear and stretching effect in the mixing process, the proportion of shear flow the particles experienced is higher than that while the tip angle is greater than 20°, and the optimal dispersive mixing performance is obtained when the tip angle is 20°. The simulation results can then be used to improve mixer design and optimize mixing stage.

Acknowledgements: This work is supported by National Natural Science Foundation of China (No.51275553). The authors would like to take this opportunity to express their sincere appreciation.

References

1. G. Böhme and O. Wünsch, *Arch. Appl. Mech.*, **67**, 167 (1997).
2. S. S. Hong, J. H. Shin, K. B. Song, and K. H. Lee, *Polym. Korea*, **37**, 342 (2013).
3. K. Shon, S. H. Bumm, and J. L. White, *Polym. Eng. Sci.*, **48**, 756 (2008).
4. T. Ishikawa, T. Amano, S. I. Kihara, and K. Funatsu, *Polym. Eng. Sci.*, **42**, 925 (2002).
5. H. Potente, K. Kretschmer, J. Hofmann, M. Senge, M. Mours, G. Scheel, and Th. Winkelmann, *Int. Polym. Proc.*, **16**, 341 (2001).
6. D. Djuric and P. Kleinebudde, *J. Pharm. Sci.*, **97**, 4934 (2008).
7. T. Brouwer, D. B. Todd, and L. Janssen, *Int. Polym. Proc.*, **17**, 26 (2002).
8. J. Wei, L. Guo, and G. H. Zhang, *J. Reinf. Plast. Compos.*, **29**, 2279 (2010).
9. J. Wei, Q. Sun, X. Sun, and W. Sun, *Int. J. Precis. Eng. Man.*, **14**, 451 (2013).
10. J. Wei, G. H. Zhang, Q. Zhang, J. S. Kim, and S. K. Lyu, *Int. J. Precis. Eng. Man.*, **9**, 59 (2008).
11. M. L. Rathod and J. L. Kokini, *J. Food Eng.*, **118** 256 (2013).
12. M. H. Kang, H. Y. Yeom, H. Y. Na, and S. J. Lee, *Polym. Korea*, **37**, 526 (2013).
13. T. Ishikawa, S. I. Kihara, and K. Funatsu, *Polym. Eng. Sci.*, **40**, 357 (2000).
14. T. Ishikawa, F. Nagano, T. Kajiwara, and K. Funatsu, *Int. Polym. Proc.*, **21**, 354 (2006).
15. M. A. Emin and H. P. Schuchmann, *J. Food Eng.*, **115**, 132 (2013).
16. T. Avalosse, Y. Rubin, and L. Fondin, *J. Reinf. Plast. Compos.*, **21**, 419 (2002).
17. B. Alsteens, V. Legat, and T. Avalosse, *Int. Polym. Proc.*, **19**, 207 (2004).
18. J. Wei, X. L. Liang, D. B. Chen, Y. L. Yang, and D. M. Zhou, *Polym. Eng. Sci.*, **54**, 2407 (2014).
19. M. L. Booy, *Polym. Eng. Sci.*, **20**, 1220 (1980).
20. T. Kajiwara, Y. Nagashima, Y. Nakano, and K. Funatsu, *Polym. Eng. Sci.*, **36**, 2142 (1996).
21. G. O. Aloku and X. F. Yuan, *Chem. Eng. Sci.*, **65**, 3749 (2010).
22. H. Cheng and I. Manas-Zloczower, *Polym. Eng. Sci.*, **38**, 926 (1998).
23. A. Kumar, G. M. Ganjyal, D. D. Jones, and M. A. Hanna, *J. Food Eng.*, **84**, 441 (2008).
24. R. K. Connelly and J. L. Kokini, *J. Food Eng.*, **79**, 956 (2007).
25. J. J. Cheng and I. Manas-Zloczower, *Int. Polym. Proc.*, **5**, 178 (1990).
26. B. J. Bentley and L. G. Leal, *J. Fluid Mech.*, **167**, 241 (1986).